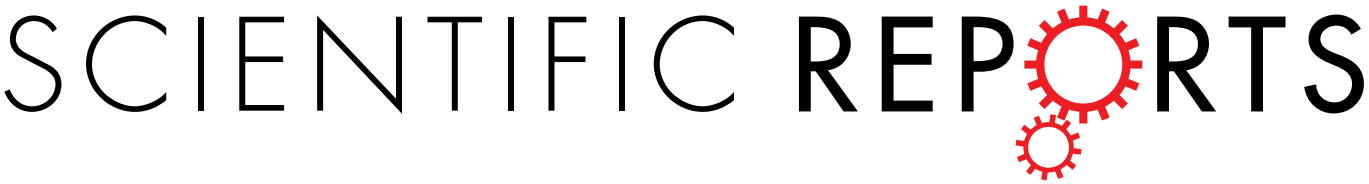

OPEN

Linear magnetoelectric effect in göthite, α-FeOOH

N. V. Ter-Oganessian[1], A. A. Guda[2] & V. P. Sakhnenko[1]

Received: 21 July 2017
Accepted: 17 November 2017
Published online: 27 November 2017

By means of symmetry analysis, density functional theory calculations, and Monte Carlo simulations we show that goethite, α-FeOOH, is a linear magnetoelectric below its Néel temperature $T_N = 400$ K. The experimentally observed magnetic field induced spin-flop phase transition results in either change of direction of electric polarization or its suppression. Estimated value of magnetoelectric coefficient is 0.57 $\mu C \cdot m^{-2} \cdot T^{-1}$. The abundance of goethite in nature makes it arguably the most widespread magnetoelectric material.

The field of multiferroics has become one of the focal points in condensed matter physics during the last two decades. Mutual influence of magnetic and electric subsystems in magnetoelectrics opens up new opportunities for practical applications such as, for example, new types of logical elements, devices for storage of information, and various sensors[1,2]. This stimulates search for new multiferroic materials both in the single-phase forms and as composites. Recent advances in the physics and design of magnetoelectrics were summarized in numerous reviews[3,4].

Magnetoelectrics are known since late 1950's and were intensively studied during the last two decades. By now, many magnetoelectric (ME) crystals or even whole classes of such compounds are identified. However, the quest for new compounds continues due to the need for higher ME coupling constants and higher working temperatures.

Iron forms many oxides and hydroxides showing a plethora of magnetic properties, which also often develop at high temperatures[5]. However, in contrast to, for example, chromium (Cr_2O_3)[6], cupric (CuO)[7], or cobalt (Co_3O_4)[8] oxides, only Fe_3O_4 and ε-Fe_2O_3 were shown to display magnetoelectric properties[9–11].

Goethite, α-FeOOH, is one of the most thermodynamically stable compounds out of iron oxides, hydroxides, or oxides-hydroxides, which arguably makes it the most abundant in nature among them[5]. It is found in rocks and soils and is often responsible for their colour. In many parts of the world current climate favours mineralogical transformation of hematite (α-Fe_2O_3) to goethite in soils and, therefore, the hematite-goethite ratio reflects the climate[12]. Goethite is also a common component of rusts, both atmospheric and electrochemical[5], and is found on Mars among other iron-containing minerals[13]. In practical use goethite is an important pigment as it is a component of ochre deposits, however it also attracts interest in the form of suspensions of nanoparticles or nanorods showing considerable magnetic field-induced birefringence[14,15].

Here we show that goethite is linear magnetoelectric below its Néel temperature $T_N = 400$ K making it (i) a room temperature ME material, and (ii) arguably the most abundant ME material known to date. Using density functional theory (DFT) we identify the main exchange coupling constants of goethite and confirm its antiferromagnetic ground state, whereas Monte Carlo studies uncover its magnetoelectric behavior in magnetic fields.

Results

Goethite, α-FeOOH, crystallizes in the orthorhombic structure with space group symmetry Pbnm (Z = 4) shown in Fig. 1(a) and lattice parameters $a = 4.55979$ Å, $b = 9.951$ Å, and $c = 3.0178$ Å[16]. Upon decreasing temperature it experiences an antiferromagnetic phase transition at temperature T_N, which varies in the range from approximately 340 to 400 K depending on the purity of the sample[17–19]. Below T_N the spins $\vec{S_i}$ of four iron ions Fe_i ($i = 1, 2, 3, 4$) located at positions (0.0489, 0.8537, 1/4), (0.9511, 0.1463, 3/4), (0.5489, 0.6463, 3/4), and (0.4511, 0.3537, 1/4)[16], order antiferromagnetically with relative spin arrangement $(+ - - +)$, respectively, as shown in Fig. 1(a)[20,21]. This ordered spin arrangement can be described by the order parameter $\vec{A}$. Other possible spin arrangements with $\vec{k} = 0$ described by the order parameters $\vec{F}$, $\vec{G}$, and $\vec{C}$ are summarized in Table 1. The direction of the ordered spins is experimentally found to be along the c axis of the crystal cell. Therefore, the appearing

[1]Institute of Physics, Southern Federal University, Rostov-on-Don, 344090, Russian Federation. [2]International Research Center "Smart Materials", Southern Federal University, Rostov-on-Don, 344090, Russia. Correspondence and requests for materials should be addressed to N.V.T.-O. (email: nikita.teroganessian@gmail.com)

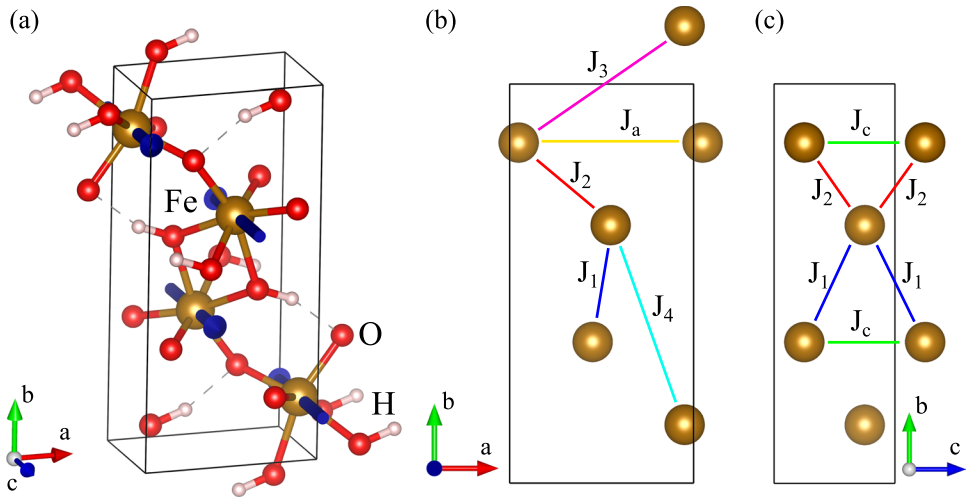

Figure 1. (**a**) Crystal and magnetic structures of α-FeOOH (blue arrows represent spins) and (**b**,**c**) magnetic exchange paths.

Fe_1	Fe_2	Fe_3	Fe_4	Order parameter	IR's
+	+	+	+	$\vec{F}$	$\Gamma^{2+}, \Gamma^{3+}, \Gamma^{4+}$
+	−	+	−	$\vec{G}$	$\Gamma^{1-}, \Gamma^{4-}, \Gamma^{3-}$
+	+	−	−	$\vec{C}$	$\Gamma^{3+}, \Gamma^{2+}, \Gamma^{1+}$
+	−	−	+	$\vec{A}$	$\Gamma^{4-}, \Gamma^{1-}, \Gamma^{2-}$

Table 1. Spin arrangements of the Fe_i ions with $\vec{k} = 0$. First four columns give relative spin orderings of Fe_i spins. The last column gives the irreducible representations (IR) according to which the components x, y, and z of the order parameters transform, respectively.

	J_1	J_2	J_3	J_4	J_a	J_c
Fe–Fe distance, Å	3.310	3.438	5.288	5.308	4.598	3.018
J, meV	15.1	48.1	−0.32	3.18	4.38	17.7

Table 2. Calculated magnetic exchange constants for α-FeOOH in meV.

magnetic structure with the wave vector $\vec{k} = 0$ can be described by the order parameter A_z. Below we adopt an orthogonal system of axes x, y, and z being parallel to the crystal axes a, b, and c, respectively.

The symmetry of magnetic structure with $A_z \neq 0$ appearing below T_N is Pb′nm[21] and allows linear magnetoelectric effect with magnetoelectric interactions given by

$$A_z F_y P_z, \tag{1}$$

$$A_z F_z P_y, \tag{2}$$

where $\vec{F}$ and $\vec{P}$ are ferromagnetic moment and electric polarization, respectively. Thus, in the antiferromagnetic phase magnetic field applied along the y or z axis induces electric polarization components P_z or P_y, respectively. It is found, however, that sufficiently strong magnetic field along the z axis results in a spin-flop transition, in which the spins reorient towards either the x or the y axis[18]. This will be discussed in more detail below.

It has to be noted here, that in the case when the initial paraelectric and paramagnetic phase possesses inversion symmetry operation, a magnetic phase transition with $\vec{k} = 0$ occurring according to a single irreducible representation cannot induce electric polarization[22]. However, linear magnetoelectric effect can be possible, as is the case in α-FeOOH: when $A_z \neq 0$ appears, the inversion symmetry is broken, but spatial inversion together with time reversal operation is a symmetry element, which results in interactions (1) and (2).

Using density functional theory we calculate six magnetic exchange constants, which are summarized in Table 2 and the respective exchange paths are shown in Fig. 1(b,c). It is found that the exchange couplings are mostly antiferromagnetic and the magnetic ground state is described by $\vec{A} \neq 0$ in accordance with the experiments.

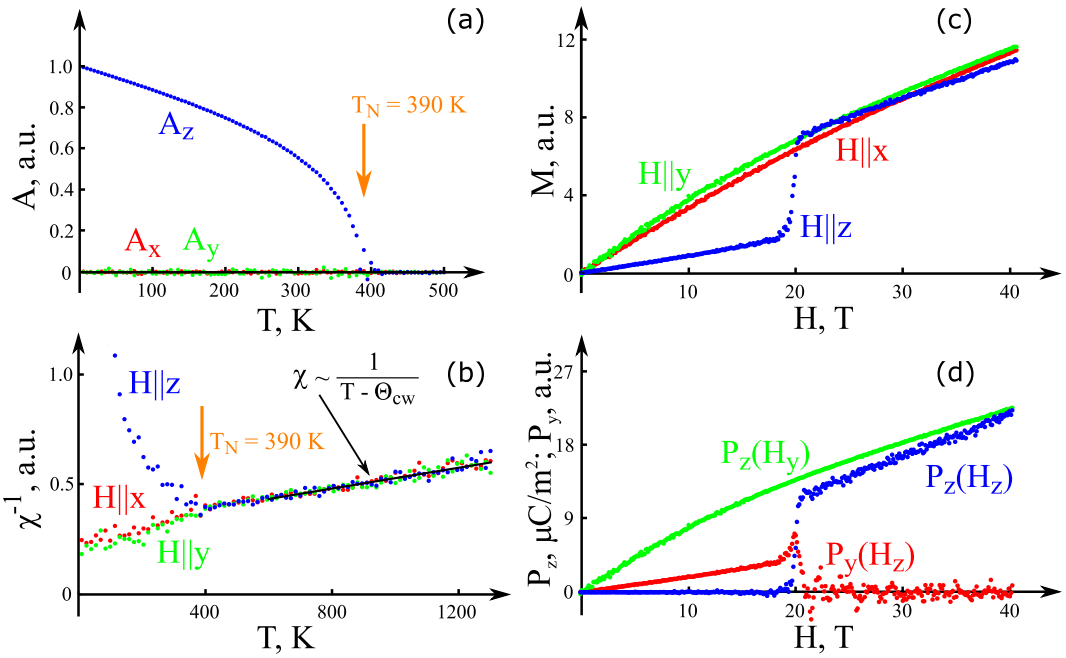

Figure 2. Results of Monte Carlo calculations. (**a**) Temperature dependence of the order parameters A_x, A_y, and A_z. (**b**) Reciprocal magnetic susceptibility for various directions as function of temperature and a fit with the Curie-Weiss law (solid line). (**c**) Magnetization and (**d**) electric polarization at $T = 100$ K as function of magnetic field.

Monte Carlo (MC) calculations reveal that with the found exchange constants the Néel temperature $T_N^{MC} = 390$ K is slightly lower than in experiments. Figure 2(a) shows temperature dependence of the order parameters, revealing that A_z emerges at T_N^{MC} confirming the appearance of antiferromagnetic order. The fit of magnetic susceptibility in the paramagnetic region by $\chi = C/(T - \Theta_{CW})$ shown in Fig. 2(b) gives the Curie-Weiss temperature $\Theta_{CW} \approx -1250$ K. This implies that in goethite considerable magnetic frustration exists since $|\Theta_{CW}|/T_N \approx 3.2$. The origin of frustration is in the presence of triangular arrangements of spins, which interact via the three dominant antiferromagnetic exchange couplings J_1, J_2, and J_c, as shown in Fig. 1(c).

At $H_c = 20$ T a spin-flop transition occurs in goethite[18] resulting in rotation of the antiferromagnetic vector to either a- or b-axis. The experimental value of the spin-flop magnetic field H_c is used to scale our results on magnetic field dependence of magnetization in the antiferromagnetic phase shown in Fig. 2(c), which are in qualitative agreement with the experimental data[18]. In our Monte Carlo simulations we assume $D_x > D_y$, which results in appearance of A_y at $H_z \geq H_c$ and corresponding vanishing of A_z.

Figure 2(d) shows H-dependence of electric polarization calculated using Eqs (1 and 2) and the ME interaction

$$A_y F_z P_z, \tag{3}$$

which is relevant in the spin-flopped phase in the case when $D_x > D_y$. (As follows from Eqs (1–3) the components of electric polarization can be calculated multiplying the components of $\vec{A}$ and $\vec{F}$ obtained by Monte Carlo simulations). It follows that in the antiferromagnetic phase α-FeOOH is a linear magnetoelectric, since external H_y and H_z induce P_z and P_y, respectively. Furthermore, at $H_z = 20$ T a flop of polarization from the b- to c-axis may occur. In the case $D_x < D_y$ the antiferromagnetic vector will flip to A_x at $H_z \geq 20$ T resulting in disappearance of electric polarization.

The microscopic origin of ME effect can be understood rewriting the ME interaction (1) through spins

$$I_1 = A_z F_y P_z = w_1 + w_2 + w_3 - w_4, \tag{4}$$

where

$$w_1 = P_z(S_{1y}S_{1z} - S_{2y}S_{2z} - S_{3y}S_{3z} + S_{4y}S_{4z}), \tag{5}$$

$$w_2 = P_z(S_{1z}S_{2y} - S_{1y}S_{2z} - S_{3z}S_{4y} + S_{3y}S_{4z}), \tag{6}$$

$$w_3 = P_z(S_{1z}S_{3y} - S_{1y}S_{3z} - S_{2z}S_{4y} + S_{2y}S_{4z}), \tag{7}$$

$$w_4 = P_z(S_{2z}S_{3y} + S_{2y}S_{3z} - S_{1z}S_{4y} - S_{1y}S_{4z}). \tag{8}$$

The interaction w_1 is a single-ion contribution, whereas w_2, w_3, and w_4 result from interactions of two spins. Thus, the ME coupling may have both single-ion and two-ion contributions. The single-ion contribution is in accordance with the local non-centrosymmetric crystal environment of Fe atoms, the local crystal symmetry of which is a mirror plane σ_z oriented parallel to the xy plane. Thus, it allows local spin-dependent electric dipole moments of electron orbitals $d_z \sim S_y S_z$[23].

In order to estimate the value of magnetically induced electric polarization we performed non-collinear DFT calculations. The spins were first relaxed in the stable A_z configuration and then constrained to give additional ferromagnetic component F_y. Artificially induced ferromagnetic ordering amounted to approximately 0.63 μ_B per spin (while the antiferromagnetic component A_z to approximately 4.09 μ_B per spin), which resulted in rotation of spins away from the z axis by about 8.8°. The resulting electric polarization calculated using the Berry phase approach was found to take the value of 120 $\mu C/m^2$. Taking the experimental magnetic susceptibility of approximately 0.003 μ_B/T per Fe^{3+} ion[24,25] we can estimate the ME coefficient to be of the order of 0.57 $\mu C \cdot m^{-2} \cdot T^{-1}$, which is comparable to that of $LiNiPO_4$[23,26].

When $D_x > D_y$ and the external magnetic field is higher than the spin-flop field $H_z > H_c$, the antiferromagnetic vector changes to $A_y \neq 0$ and P_z appears. DFT calculations in this phase give value of the ME coefficient $\partial P_z/\partial H_z$ very close to the value of $\partial P_z/\partial H_y$ in the phase $A_z \neq 0$ calculated above. These ME coefficients together with the spin-flop field value allow to set scaling of P_z and magnetic field in Fig. 2(d). However, the ME coefficient $\partial P_y/\partial H_z$ in the low field phase $A_z \neq 0$ depends on the unknown magnetic susceptibility $\chi_{\parallel} = \partial M_z/\partial H_z$, which should be much lower, though, than $\chi_{\perp} = \partial M_y/\partial H_y$, precluding from setting reliable scale for P_y in Fig. 2(d).

Relative values of different contributions to ME effect can be estimated from DFT calculations. For this purpose one can use the ME interactions

$$I_2 = C_z G_y P_z = w_1 - w_2 + w_3 + w_4, \tag{9}$$

$$I_3 = A_y F_z P_z = w_1 - w_2 - w_3 - w_4, \tag{10}$$

$$I_4 = C_y G_z P_z = w_1 + w_2 - w_3 + w_4. \tag{11}$$

Performing calculations using the magnetic configurations $C_z C_y$, $A_y F_z$, and $C_z C_y$ similar to above and evaluating P_z using the Berry phase approach we find that the biggest contribution to ME effect is w_3 and the other contributions relative to w_3 are $w_1/w_3 \approx -0.034$, $w_2/w_3 \approx -0.21$, and $w_4/w_3 = 0$. Therefore, it follows that w_1 and w_2 act in the direction opposite to w_3.

Conclusions

Based on the symmetry analysis of the available crystal and magnetic structures of goethite, α-FeOOH, we suggest that it is linear magnetoelectric below its Néel temperature. Using density functional calculations and Monte Carlo simulations we find main exchange constants in goethite and calculate its magnetic and magnetoelectric behavior.

Goethite belongs to the α-AlOOH diaspore structural type, which is also shared by, for example, α-MnOOH, Fe(OH)F, and Co(OH)F. The latter compound is also antiferromagnetic below ~40 K with the spin arrangement similar to α-FeOOH[27] and should, thus, display similar linear ME properties below its T_N.

Nature creates beautiful polycrystalline goethite samples, which are encountered in significant amounts in various deposits. However, synthesis of single crystals in laboratory or preparation of good ceramic samples can be a challenge, as α-FeOOH starts to decompose at temperatures higher than 200 °C to form hematite, α-Fe_2O_3 In this respect it may be easier to show the magnetoelectric behavior experimentally in the aforementioned isostructural compounds with similar magnetic structure, e.g., in Co(OH)F.

Methods

DFT calculations. Density functional theory calculations were performed using the Vienna *Ab-initio* Simulation Package (VASP)[28] and the projected augmented wave method[29]. We used the GGA exchange correlation approximation corrected by means of the GGA + U formalism for the Fe atoms with $U_{eff} = U - J = 3$ eV within the Dudarev approach[30]. This value of U_{eff} was shown earlier to properly account for the structural and magnetic properties of α-FeOOH[31,32]. The energy cutoff was 850 eV, whereas the Brillouin zone integration was done using the $8 \times 4 \times 12$ set of k-points determined by the Monkhorst-Pack scheme, which provided both the energy and k-points convergence.

Spin polarized collinear calculations were used to determine the exchange constants. For the determination of 6 exchange couplings the Hamiltonian was fitted to relative total energies of 7 different collinear magnetic structures. Magnetic cell sizes included $a \times b \times c$, $2a \times b \times c$, $a \times b \times 2c$, and $2a \times 2b \times c$, with the corresponding changes in the k-points grid. The crystal structure was relaxed in the most stable $\overrightarrow{A}$ magnetic structure using the stopping criterion for absolute values of forces on atoms of 10^{-3} eV/Å, while fixing the atomic positions for total energy calculations of other magnetic structures.

Electric polarization was calculated using the Berry phase approach as implemented in VASP while including spin-orbit coupling and performing fully non-collinear magnetic calculations. Since electric polarization appears in non-collinear magnetic structures the directions of local magnetic moments were constrained to form slightly non-collinear magnetic structure, while allowing for atomic and structural relaxation.

The calculated lattice parameters $a = 4.638$ Å, $b = 10.037$ Å, and $c = 3.038$ Å are within 1% of the experimentally determined values[16,21]. The local magnetic moment value of 4.14 μ_B of Fe ions is between the experimentally

reported values of 3.8 μ_B[33] and 4.45 μ_B[21]. The band gap 1.9 eV obtained in DFT calculations is slightly lower than the experimental values 2.1–2.5 eV[34,35].

Classical Monte-Carlo simulations. Classical Monte Carlo simulations using the exchange constants determined by DFT calculations are performed using the Hamiltonian

$$\mathcal{H} = \sum_{ij} J_{ij} \overrightarrow{S_i} \cdot \overrightarrow{S_j} + \sum_i (D_x S_{ix}^2 + D_y S_{iy}^2 + D_z S_{iz}^2) - \overrightarrow{H} \cdot \overrightarrow{S}, \tag{12}$$

where $\overrightarrow{S}$ are classical vectors of unit length, D_α ($\alpha = x, y, z$) are anisotropy constants, and $\overrightarrow{H}$ is magnetic field. In the Hamiltonian (12) we account only for the anisotropy terms $D_\alpha \neq 0$ pursuing a minimal model, which reproduces the ground state $A_z \neq 0$. However, it has to be noted that there exist other anisotropy terms, which can generate some *G*-type contribution to the magnetic structure in the spin-flopped phase (i.e., when $A_x \neq 0$ or $A_y \neq 0$) when magnetic field is applied along the z direction, but not in the ground state, since A_z is the only order parameter transforming according to the irreducible representation Γ^{2-}. We assume that such interactions are small and will only slightly modify the results quantitatively. In our simulations we tentatively use $D_x = -D_z = 1.5$ meV and $D_y = 0$, which reflects the easy axis direction parallel to the *c*-axis.

The calculations are performed using the Metropolis scheme and a simulation box with dimensions $12 \times 12 \times 12$ unit cells. After every change in temperature or external magnetic field the system is allowed to relax for $5 \cdot 10^3$ Monte Carlo steps per spin (MCS), whereas the statistical information is subsequently gathered over the next $15 \cdot 10^3$ MCS. Simulations of larger systems with dimensions $18 \times 18 \times 18$ and $24 \times 24 \times 24$ resulted in only slight increase of T_N by approximately 2% and 3%, respectively.

References

1. Scott, J. F. Applications of magnetoelectrics. *J. Mater. Chem.* **22**, 4567–4574 (2012).
2. Ortega, N., Kumar, A., Scott, J. F. & Katiyar, R. S. Multifunctional magnetoelectric materials for device applications. *J. Phys.: Condens. Matter* **27**, 504002 (2015).
3. Dong, S., Liu, J.-M., Cheong, S.-W. & Ren, Z. Multiferroic materials and magnetoelectric physics: symmetry, entanglement, excitation, and topology. *Adv. Phys.* **64**, 519–626 (2015).
4. Young, J., Stroppa, A., Picozzi, S. & Rondinelli, J. M. Anharmonic lattice interactions in improper ferroelectrics for multiferroic design. *J. Phys.: Condens. Matter* **27**, 283202 (2015).
5. Cornell, R. M. & Schwertmann, U. *The Iron Oxides: Structure, Properties, Reactions, Occurences and Uses* (WILEY-VCH Verlag, Weinheim, 2003).
6. Astrov, D. N. The magnetoelectric effect in antiferromagnetics. *JETP* **11**, 708–709 (1960).
7. Kimura, T., Sekio, Y., Nakamura, H., Siegrist, T. & Ramirez, A. P. Cupric oxide as an induced-multiferroic with high-T_c. *Nat. Mater.* **7**, 291–294 (2008).
8. Saha, R. *et al.* Magnetoelectric effect in simple collinear antiferromagnetic spinels. *Phys. Rev. B* **94**, 014428 (2016).
9. Kita, E. *et al.* Magnetoelectric effect of Fe_3O_4 at 77 K. II. Electric field dependence of magnetic anisotropy. *J. Phys. Soc. Jpn.* **47**, 1788–1796 (1979).
10. Yamauchi, K., Fukushima, T. & Picozzi, S. Ferroelectricity in multiferroic magnetite Fe_3O_4 driven by noncentrosymmetric Fe^{2+}/Fe^{3+} charge-ordering: first-principles study. *Phys. Rev. B* **79**, 212404 (2009).
11. Gich, M. *et al.* Magnetoelectric coupling in ε-Fe_2O_3 nanoparticles. *Nanotechnology* **17**, 687–691 (2006).
12. Schwertmann, U. Transformation of hematite to goethite in soils. *Nature* **232**, 624–625 (1971).
13. Morris, R. V. *et al.* Iron mineralogy and aqueous alteration from Husband Hill through Home Plate at Gusev Crater, Mars: Results from the Mössbauer instrument on the Spirit Mars Exploration Rover. *J. Geophys. Res.* **113**, E12S42 (2008).
14. Lemaire, B. J. *et al.* Outstanding magnetic properties of nematic suspensions of goethite (α-FeOOH) nanorods. *Phys. Rev. Lett.* **88**, 125507 (2002).
15. Li, J. *et al.* Large magneto-optical birefringence of colloidal suspensions of α-FeOOH goethite nanocrystallites. *Chem. Phys. Lett.* **590**, 168–168 (2013).
16. Yang, H., Lu, R., Downs, R. T. & Costin, G. Goethite, α-FeO(OH), from single-crystal data. *Acta Cryst. E* **62**, i250–i252 (2006).
17. De Grave, E. & Vandenberghe, R. E. ^{57}Fe Mössbauer effect study of well-crystallized goethite (α-FeOOH). *Hyper. Interactions* **28**, 643–646 (1986).
18. Coey, J. M. D. *et al.* Spin flop in goethite. *J. Phys.: Condens. Matter* **7**, 759–768 (1995).
19. Bocquet, S. & Hill, A. J. Correlation of Néel temperature and vacancy defects in fine-particle goethites. *Phys. Chem. Miner.* **22**, 524–528 (1995).
20. Forsyth, J. B., Hedley, I. G. & Johnson, C. E. The magnetic structure and hyperfine field of goethite (α-FeOOH). *J. Phys. C: Solid State Phys.* **1**, 179–188 (1968).
21. Zepeda-Alarcon, E. *et al.* Magnetic and nuclear structure of goethite (α-FeOOH): a neutron diffraction study. *J. Appl. Cryst.* **47**, 1983–1991 (2014).
22. Kovalev, O. V. Antiferromagnets with electric polarization. *Sov. Phys. Cryst.* **18**, 137–140 (1973).
23. Sakhnenko, V. P. & Ter-Oganessian, N. V. The magnetoelectric effect due to local noncentrosymmetry. *J. Phys.: Condens. Matter* **24**, 266002 (2012).
24. Martin-Hernandez, F. & García-Hernández, M. M. Magnetic properties and anisotropy constant of goethite single crystals at saturating high fields. *Geophys. J. Int.* **181**, 756–761 (2010).
25. Pankhurst, Q. A., Barquín, L. F., Lord, J. S., Amato, A. & Zimmermann, U. Intrinsic magnetic relaxation in goethite. *Phys. Rev. B* **85**, 174437 (2012).
26. Kornev, I. *et al.* Magnetoelectric properties of $LiCoPO_4$ and $LiNiPO_4$. *Phys. Rev. B* **62**, 12247–12253 (2000).
27. Yahia, H. B. *et al.* Synthesis and characterization of the crystal and magnetic structures and properties of the hydroxyfluorides Fe(OH)F and Co(OH)F. *Inorg. Chem.* **53**, 365–374 (2014).
28. Kresse, G. & Furthmüller, J. Efficient iterative schemes for *ab initio* total-energy calculations using a plane-wave basis set. *Phys. Rev. B* **54**, 11169–11186 (1996).
29. Blöchl, P. E. Projector augmented-wave method. *Phys. Rev. B* **50**, 17953–17979 (1994).
30. Dudarev, S. L., Botton, G. A., Savrasov, S. Y., Humphreys, C. J. & Sutton, A. P. Electron-energy-loss spectra and the structural stability of nickel oxide: An LSDA + U study. *Phys. Rev. B* **57**, 1505–1509 (1998).
31. Tunega, D. Theoretical study of properties of goethite (α-FeOOH) at ambient and high-pressure conditions. *J. Phys. Chem. C* **116**, 6703–6713 (2012).

32. Meng, Y. *et al*. When density functional approximations meet iron oxides. *J. Chem. Theory Comput.* **12**, 5132–5144 (2016).
33. Bocquet, S. & Kennedy, S. J. The Néel temperature of fine particle goethite. *J. Magn. Magn. Mater.* **109**, 260–264 (1992).
34. Leland, J. K. & Bard, A. J. Photochemistry of colloidal semiconducting iron oxide polymorphs. *J. Phys. Chem.* **91**, 5076–5083 (1987).
35. Sherman, D. M. Electronic structures of iron(III) and manganese(IV) (hydr)oxide minerals: Thermodynamics of photochemical reductive dissolution in aquatic environments. *Geochim. Cosmochim. Acta* **69**, 3249–3255 (2005).

Acknowledgements

N.V.T. acknowledges financial support by the RA MES SCS, within the frames of the "RA MES SCS - YSU - RF SFEDU" international call for joint project No. VnGr-07/2017-32.

Author Contributions

N.V.T. conceived the project. A.A.G. performed DFT calculations. N.V.T. did the Monte Carlo simulations. N.V.T. and V.P.S. supervised the research and wrote the manuscript. All authors discussed the results and commented on the manuscript.

Additional Information

Competing Interests: The authors declare that they have no competing interests.

Publisher's note: Springer Nature remains neutral with regard to jurisdictional claims in published maps and institutional affiliations.